Corrected 7 February 2023. See full text.

RESEARCH ARTICLE SUMMARY

CANCER GENOMICS

Chromatin profiles classify castration-resistant prostate cancers suggesting therapeutic targets

Fanying Tang†, Duo Xu†, Shangqian Wang†, Chen Khuan Wong†, Alexander Martinez-Fundichely, Cindy J. Lee, Sandra Cohen, Jane Park, Corinne E. Hill, Kenneth Eng, Rohan Bareja, Teng Han, Eric Minwei Liu, Ann Palladino, Wei Di, Dong Gao, Wassim Abida, Shaham Beg, Loredana Puca, Maximiliano Meneses, Elisa de Stanchina, Michael F. Berger, Anuradha Gopalan, Lukas E. Dow, Juan Miguel Mosquera, Himisha Beltran, Cora N. Sternberg, Ping Chi, Howard I. Scher, Andrea Sboner, Yu Chen*, Ekta Khurana*

INTRODUCTION: Untreated prostate cancers rely on androgen receptor (AR) signaling for growth and survival, forming the basis for the initial efficacy of androgen deprivation therapy (ADT). Yet the disease can relapse and progress to a lethal stage termed castration-resistant prostate cancer (CRPC). Reactivation of AR signaling represents the most common driver of CRPC growth, and next-generation AR signaling inhibitors (ARSIs) are now used in combination with ADT as a first-line therapy. However, ARSIs can result in selective pressure, thereby generating AR-independent tumors. The transition from AR dependence frequently accompanies a change in phenotype resembling developmental transdifferentiation or "lineage plasticity." Neuroendocrine prostate cancer, which lacks a defined pathologic classification, is the most studied type of lineage plasticity. However, most AR-null tumors do not exhibit neuroendocrine features and are classified as "double-negative prostate cancer," the drivers of which are poorly defined.

RATIONALE: Lineage plasticity studies in CRPC are limited by the lack of genetically defined patient-derived models that recapitulate the disease spectrum. To address this, we developed a biobank of organoids generated from patient biopsies to study the landscape of metastatic CRPC and allow for functional validation assays. Proteins called transcription factors (TFs) are drivers of tumor lineage plasticity. To identify the key TFs that drive the growth of AR-independent tumors, we integrated epigenetic and transcriptomic data generated from CRPC models.

RESULTS: We generated ATAC-seq (assay for transposase-accessible chromatin sequencing) and RNA-seq data from 22 metastatic human prostate cancer organoids, six patient-derived xenografts (PDXs), and 12 derived or traditional cell lines. We classified the 40 models into four subtypes and predicted key TFs of each subtype. We identified the well-characterized AR-dependent (CRPC-AR) and neuroendocrine subtypes (CRPC-NE) as well as two AR-negative/low groups, including a Wnt-dependent subtype (CRPC-WNT), driven by TCF/LEF TFs, and a stem cell–like (SCL) subtype (CRPC-SCL), driven by the AP-1 family of TFs. We applied RNA-seq signatures derived from the organoids to 366 patient samples from two independent CRPC datasets, which recapitulated the four-subtype classification. We found that CRPC-SCL is the second most prevalent group and is associated with shorter time under ARSI treatment compared to CRPC-AR. Additional chromatin immunoprecipitation sequencing (ChIP-seq) analysis indicated that AP-1 works together with the proteins YAP, TAZ, and TEAD, revealing YAP/TAZ and AP-1 as potential actionable targets in CRPC-SCL. Using overexpression assays in AR-high cells, we revealed how AP-1 functions as a pioneering factor and master regulator for CRPC-SCL.

CONCLUSION: By using a diverse biobank of organoids, PDXs, and cell lines that recapitulate the heterogeneity of metastatic prostate cancer, we created a map of the chromatin accessibility and transcriptomic landscape of CRPC. We validated the CRPC-AR and CRPC-NE subtypes and report two subtypes of AR-negative/low samples as well as their respective key TFs. Additional analysis revealed a model in which YAP, TAZ, TEAD, and AP-1 function together and drive oncogenic growth in CRPC-SCL samples. Overall, our results show how stratification of CRPC patients into four subtypes using their transcriptomes can potentially inform appropriate clinical decisions. ■

The list of author affiliations is available in the full article online.
*Corresponding author. Email: ekk2003@med.cornell.edu (E.K.); cheny1@mskcc.org (Y.C.)
†These authors contributed equally to this work.
Cite this article as F. Tang *et al.*, *Science* **376**, eabe1505 (2022). DOI: 10.1126/science.abe1505

READ THE FULL ARTICLE AT
https://doi.org/10.1126/science.abe1505

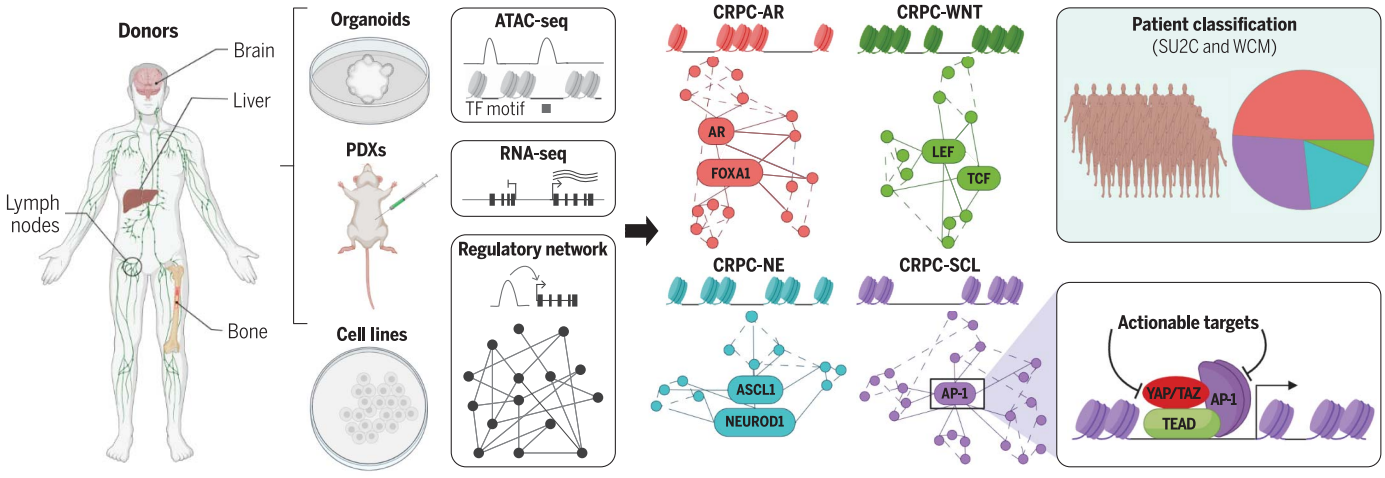

Identification of four subtypes of castration-resistant prostate cancer (CRPC) by integration of chromatin accessibility and transcriptomic data from organoids, patient-derived xenografts (PDXs), and cell lines. TF, transcription factor; AR, androgen receptor; NE, neuroendocrine; SCL, stem cell–like. YAP/TAZ/TEAD/AP-1 cooperation in CRPC-SCL suggests actionable targets. Application of RNA-seq signatures derived from the models to 366 patient samples recapitulates the four-subtype classification.

Corrected 7 February 2023. See full text.

RESEARCH ARTICLE

CANCER GENOMICS

Chromatin profiles classify castration-resistant prostate cancers suggesting therapeutic targets

Fanying Tang[1,2]†‡, Duo Xu[1,2,3,4]†, Shangqian Wang[5,6]†, Chen Khuan Wong[5]†, Alexander Martinez-Fundichely[1,2,3,4], Cindy J. Lee[5], Sandra Cohen[1], Jane Park[7], Corinne E. Hill[7], Kenneth Eng[4]§, Rohan Bareja[4], Teng Han[5], Eric Minwei Liu[1,2,8], Ann Palladino[1,2], Wei Di[5], Dong Gao[5,9], Wassim Abida[10], Shaham Beg[4], Loredana Puca[1,4]¶, Maximiliano Meneses[11], Elisa de Stanchina[11], Michael F. Berger[12], Anuradha Gopalan[12], Lukas E. Dow[1,13], Juan Miguel Mosquera[1,4,14], Himisha Beltran[4,15], Cora N. Sternberg[1,4], Ping Chi[5,10,13], Howard I. Scher[10,16], Andrea Sboner[2,4,14], Yu Chen[5,10,13]*, Ekta Khurana[1,2,3,4]*

In castration-resistant prostate cancer (CRPC), the loss of androgen receptor (AR) dependence leads to clinically aggressive tumors with few therapeutic options. We used ATAC-seq (assay for transposase-accessible chromatin sequencing), RNA-seq, and DNA sequencing to investigate 22 organoids, six patient-derived xenografts, and 12 cell lines. We identified the well-characterized AR-dependent and neuroendocrine subtypes, as well as two AR-negative/low groups: a Wnt-dependent subtype, and a stem cell–like (SCL) subtype driven by activator protein–1 (AP-1) transcription factors. We used transcriptomic signatures to classify 366 patients, which showed that SCL is the second most common subtype of CRPC after AR-dependent. Our data suggest that AP-1 interacts with the YAP/TAZ and TEAD proteins to maintain subtype-specific chromatin accessibility and transcriptomic landscapes in this group. Together, this molecular classification reveals drug targets and can potentially guide therapeutic decisions.

Untreated prostate cancers rely on androgen receptor (AR) signaling for growth and survival, forming the basis for the initial efficacy of androgen deprivation therapy (ADT). Yet the disease can relapse and progress to a lethal stage termed castration-resistant prostate cancer (CRPC). Reactivation of AR signaling represents the most common driver of CRPC growth, and next-generation AR signaling inhibitors (ARSIs) are now used in combination with ADT as a first-line therapy (*1*). However, ARSIs can also result in selective pressure, thereby generating AR-independent tumors. The transition from AR dependence frequently accompanies a change in phenotype that resembles developmental transdifferentiation or "lineage plasticity" (*2*). Neuroendocrine prostate cancer (NEPC), which lacks a defined pathologic classification, is the most studied type of lineage plasticity (*3*, *4*). However, most AR-null tumors do not exhibit neuroendocrine features and are classified as "double-negative prostate cancer" (DNPC), the drivers of which are poorly defined (*5*, *6*).

Mechanistic studies in CRPC are limited by the lack of genetically defined patient-derived models that recapitulate the disease spectrum. To address this, we have developed a biobank of organoids generated from patient biopsies to study the landscape of metastatic CRPC and allow for functional validation assays (*7*, *8*).

Biobank of patient-derived organoids of metastatic CRPC

We generated and characterized 15 organoids from specimens of patients with metastatic prostate cancer (MSKPCa8-MSKPCa20, MSKPCa22, MSKPCa24), adding to our biobank of seven organoids (*7*, *8*). In general, the organoids were from patients with aggressive disease, short response to initial ADT, and rapid progression following second-line treatment with an ARSI (table S1). In culture, the organoids adopted histology similar to the tissues from which they were developed (fig. S1, A and B), and the neuroendocrine samples maintained immunohistochemistry staining of synaptophysin (SYP) (fig. S1C).

We generated mutational and copy number profiles of each organoid, as well as 10 of 15 matching tumor biopsy specimens, using MSK-IMPACT (Memorial Sloan Kettering–Integrated Mutation Profiling of Actionable Cancer Targets) (*9*). The copy number landscape was similar between tumors and organoids and was representative of metastatic CRPC when compared to the Stand Up to Cancer (SU2C) cohort (*10*) (Fig. 1A). We observed a mean of 3.6 somatic mutations per patient, similar to the cohort of metastatic prostate cancer patients profiled using MSK-IMPACT (*9*) (Fig. 1B). The majority of organoids exhibited the same copy number variations (CNVs) and single-nucleotide variants (SNVs) as the original biopsies (fig. S1D and tables S2 and S3). In fact, organoids contained a higher fraction of tumor cells than the original biopsies, as shown by the increased allelic frequency of SNVs and CNVs (Fig. 1A and table S2).

Chromatin accessibility landscape reveals four molecular subtypes of metastatic prostate cancer

We performed ATAC-seq (assay for transposase-accessible chromatin sequencing) assays for 35 metastatic prostate cancer models, including 22 patient-derived organoids, six patient-derived xenografts (PDXs), and seven cell lines (two biological replicates for each) (fig. S2, A to E, and table S4). We also included published ATAC-seq data from five NEPC models (*11*) (Fig. 1C). Overall, we identified 861,195 reproducible peaks. The majority of the ATAC-seq peaks mapped to distal intergenic and intronic regions, similar to reports by other groups (*12*) (Fig. 1C). We identified four CRPC subtypes using consensus k-means clustering on the regions showing the most variable accessibility (fig. S2, F to H). We obtained the same four groups using other approaches, such as hierarchical clustering and UMAP (uniform manifold approximation and projection) (Fig. 1, D and E). There was no significant difference between the numbers of peaks among the four subtypes (fig. S2I, two-sided Wilcoxon rank-sum

[1]Sandra and Edward Meyer Cancer Center, Weill Cornell Medicine, New York, NY 10021, USA. [2]Institute for Computational Biomedicine, Weill Cornell Medical College, New York, NY 10021, USA. [3]Department of Physiology and Biophysics, Weill Cornell Medical College, New York, NY 10021, USA. [4]Englander Institute for Precision Medicine, Weill Cornell Medicine, New York, NY 10021, USA. [5]Human Oncology and Pathogenesis Program, Department of Medicine, Memorial Sloan Kettering Cancer Center, New York, NY 10065, USA. [6]State Key Laboratory of Reproductive Medicine, Urology Department, First Affiliated Hospital of Nanjing Medical University, Nanjing 211116, China. [7]Center for Epigenetics Research, Memorial Sloan Kettering Cancer Center, New York, NY 10065, USA. [8]Computational Oncology Service, Memorial Sloan Kettering Cancer Center, New York, NY 10065, USA. [9]State Key Laboratory of Cell Biology, Shanghai Key Laboratory of Molecular Andrology, Shanghai Institute of Biochemistry and Cell Biology, Center for Excellence in Molecular Cell Science, Chinese Academy of Sciences, Shanghai 200031, China. [10]Department of Medicine, Memorial Sloan Kettering Cancer Center, New York, NY 10065, USA. [11]Antitumor Assessment Core Facility, Memorial Sloan Kettering Cancer Center, New York, NY 10065, USA. [12]Department of Pathology, Memorial Sloan Kettering Cancer Center, New York, NY 10065, USA. [13]Department of Medicine, Weill Cornell Medical College and New York–Presbyterian Hospital, New York, NY 10065, USA. [14]Department of Pathology and Laboratory Medicine, Weill Cornell Medical College, New York, NY 10065, USA. [15]Department of Medical Oncology, Dana-Farber Cancer Institute, Boston, MA 02215, USA. [16]Biomarker Development Program, Memorial Sloan Kettering Cancer Center, New York, NY 10065, USA.
*Corresponding author. Email: ekk2003@med.cornell.edu (E.K.); cheny1@mskcc.org (Y.C.) †These authors contributed equally to this work.
‡Present address: AbbVie Cambridge Research Center, Cambridge, MA 02139, USA. §Present address: Illumina Inc., San Diego, CA 92122, USA.
¶Present address: Loxo Oncology at Lilly, New York, NY 10016, USA.

Corrected 7 February 2023. See full text.

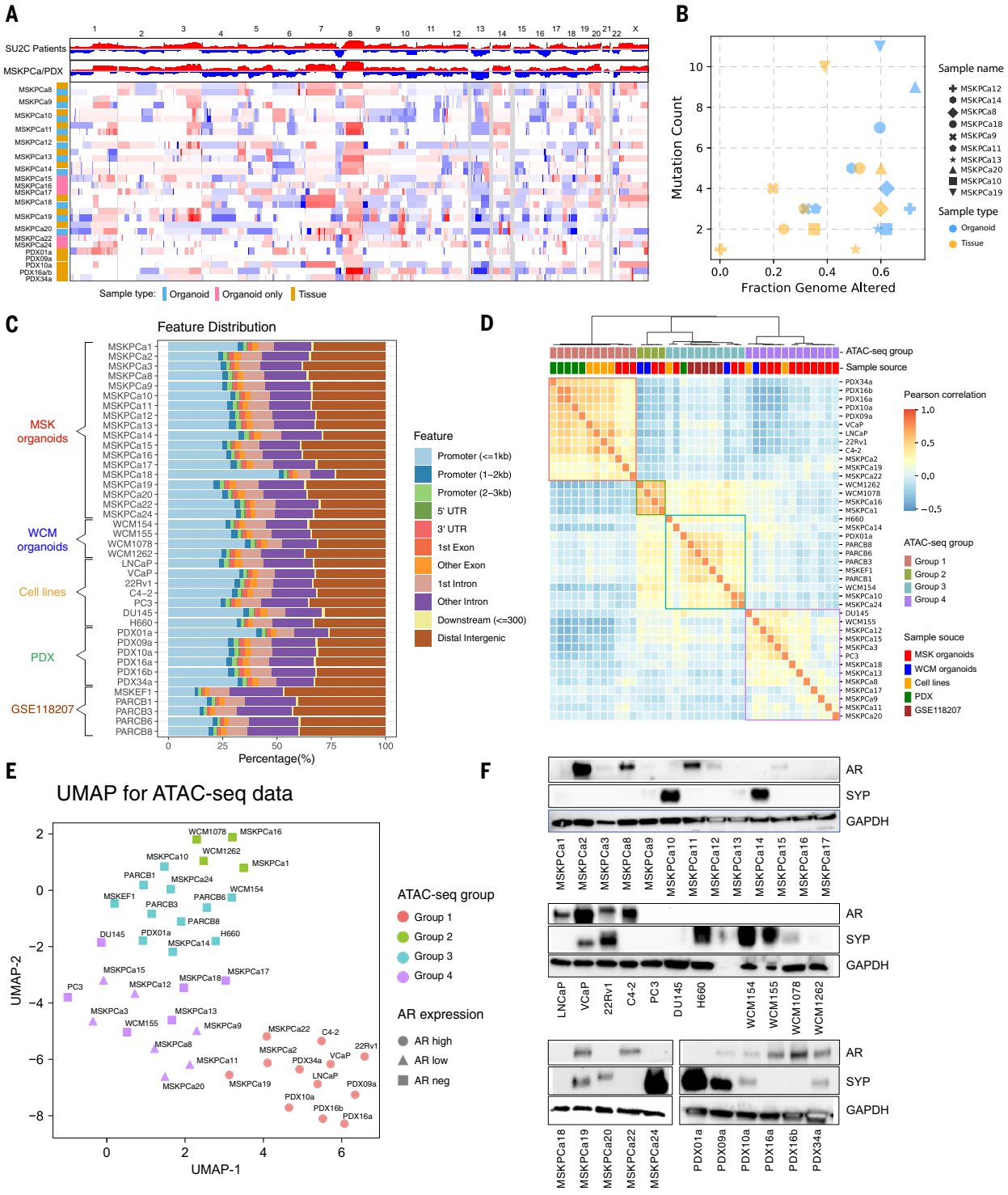

Fig. 1. Classification of metastatic prostate cancer into four molecular subtypes from chromatin accessibility. (**A**) Top: Genomic aberrations in the prostate oncogenome from the SU2C CRPC patient samples (*10*) and MSKPCa organoids. Bottom: Copy number landscape of the 15 patient-derived organoid lines and 10 matching tumor tissues using MSK-IMPACT sequencing data. Shades of red and blue represent extent of gain and loss. (**B**) Number of mutations and fraction of copy number–altered genome of the 10 organoids and their matching patient tumor tissues. (**C**) Feature distribution of the mapped ATAC-seq peaks across all samples. (**D**) Correlation heatmap based on the normalized number of reads of the top 1% variable peaks across all samples. The ATAC-seq group and the sample source are indicated for each sample. The colors of the four ATAC-seq groups are kept consistent throughout the paper. (**E**) Unsupervised UMAP on the top 1% variable accessible peaks across all samples. (**F**) Immunoblot showing the expression of AR, SYP, and GAPDH (control) across the 35 organoids, PDXs, and cell lines.

Corrected 7 February 2023. See full text.

test). The signature peaks for each subtype, defined as those with $\log_2$(fold change) > 2 and $P < 0.01$, were enriched at enhancers relative to promoters ($P = 4.18 \times 10^{-126}$, one-tailed Fisher's exact test), consistent with reports that the enhancer landscape better reflects cell identity than promoter accessibility (table S5) (*13*).

One of the four subtypes consisted of high AR-expressing samples, including the cell lines LNCaP, VCaP, 22Rv1, and C4-2; the organoids MSKPCa2, MSKPCa19, and MSKPCa22; and five PDXs (Fig. 1F). All these samples showed increased chromatin accessibility at AR target genes such as *KLK2* (fig. S2J). Another subtype included published NEPC samples H660, WCM154, PARCB1, PARCB3, PARCB6, PARCB8, and MSKEF1 (a derivative of published neuroendocrine organoid MSKPCa4); three new organoid lines, MSKPCa10, MSKPCa14, and MSKPCa24; and one PDX model with high SYP expression and small-cell carcinoma phenotype (Fig. 1F and fig. S1, A and C). The remaining two subtypes consisted of neuroendocrine-negative (NE-negative) and AR-negative/low samples (Fig. 1, E and F). For further biological characterization, we integrated the ATAC-seq data with RNA-seq and DNA sequencing data.

Transcriptomic profiles of the four CRPC subtypes

We next analyzed the transcriptomes of the 40 samples using UMAP and found that the clusters agree with the subtypes identified using ATAC-seq (Fig. 2A). Gene set enrichment analysis (GSEA) and selective marker gene expression (Fig. 2, B and C, and fig. S3, A to C) were used to name the four subtypes as follows: (i) CRPC-AR, which is enriched in the AR signature (*14*); (ii) CRPC-WNT, which is enriched in Wnt signaling and includes the organoids WCM1078, WCM1262, MSKPCa1, and MSKPCa16; (iii) CRPC-NE, which is enriched in the NE signature (*15*) in agreement with the pathology classification (fig. S1, A and C) and has high expression of NE markers, including SYP, CHGA, and DLL3; and (iv) CRPC-SCL, consisting of stem cell–like (SCL) samples, including 11 organoids and cell lines DU145 and PC3.

CRPC-SCL has not been previously identified. Samples in this subtype were enriched in the mammary stem cell signature, with high expression of the cancer stem cell markers CD44 and TACSTD2 (TROP2A) (Fig. 2, B and C, and fig. S3, A and B). Samples in CRPC-SCL were also enriched in pathways involving interleukin-6/Janus kinase/signal transducer and activator of transcription 3, transforming growth factor–β, tumor necrosis factor–α signaling, epithelial-mesenchymal transition, inflammation, and interferon response (fig. S4A).

Relative to CRPC-AR, the other three groups were enriched with a basal signature (*16*) and prostate basal stem cell signature (*17*), with CRPC-SCL exhibiting the highest enrichment score (fig. S4B) and expression of basal cell markers (Fig. 2C). In addition, consistent with previous studies of AR-negative/low tumors, CRPC-WNT and CRPC-SCL showed enrichment of fibroblast growth factor receptor (FGFR) signaling and expression of selective FGF ligands and receptors compared to the other two groups (fig. S5, A and B) (*5*).

Genomic characterization and loss of tumor suppressors in the four CRPC subtypes

Samples in CRPC-AR were enriched for AR amplification and/or AR mutation (Fig. 2D; $P = 7.01 \times 10^{-6}$, one-tailed Fisher's exact test). In CRPC-WNT, all four samples showed alterations in the Wnt signaling pathway (*18*) (Fig. 2D and fig. S5C). Three CRPC-WNT samples showed hot spot mutations in CTNNB1 (β-catenin) (Fig. 2D and fig. S5C). The fourth sample had shallow deletion of APC and gain of RSPO2 (*18*) (fig. S5C).

Loss of the tumor suppressors TP53, PTEN, and RB1 is associated with lineage plasticity and aggressive disease in CRPC (*16*, *19*). We found that *TP53* was the most frequently mutated gene, with putative driver mutations or deep deletions in 23 of 35 samples (66%) across all four groups. *RB1* and *PTEN* had biallelic alterations in 20% and 43% of samples, respectively (Fig. 2D and fig. S5D). Using RNA-seq and immunoblot analysis, we found that an additional 11 of 35 samples (31.4%) exhibited RB1 loss, and 10 of 35 samples (28.5%) exhibited PTEN loss (table S6 and figs. S5E and S6). Overall, we found an enrichment of RB1 loss in AR-negative/low samples (14 of 24) compared to CRPC-AR (2 of 12) ($P = 0.0200$, one-tailed Fisher's exact test); there was no statistical difference in *PTEN* and *TP53* alterations between CRPC-AR and others. AR-independent CRPC has worse prognosis, and thus these results agree with recent studies indicating that *RB1* alterations, but not *TP53* and *PTEN* alterations, are associated with shorter survival in CRPC (*20*, *21*). It is notable that although 11 of 24 lines exhibited loss of both *TP53* and *RB1* in the AR-negative/low samples, only three were overtly NEPC (fig. S1, A to C), consistent with recent observations that loss of *TP53* and *RB1* in prostate carcinoma attenuates AR signaling but does not uniformly induce the neuroendocrine phenotype (*22*). This further highlights the importance of transcriptomic and epigenetic analysis in defining CRPC subtypes.

Construction of regulatory networks and identification of key TFs

To identify the key TFs that drive the subtype-specific transcriptome, we first identified the hubs in regulatory networks that target a large number of genes in a given sample (*23*). We constructed regulatory networks by integrating ATAC-seq and RNA-seq data, and built the peak-gene links based on the correlation between chromatin accessibility at ATAC-seq peaks and expression of genes within ±0.5 Mb (Fig. 3A, step 1) (*12*, *24*). In total, we identified at least one peak-gene link for 4752 protein-coding genes (table S7). We predicted that 75.2% of the peaks regulate only one gene, and on average the expression of one gene was correlated with the activity of three peaks (Fig. 3, B and C). To uncover TF-DNA binding sites in the accessible regions, we used a footprinting method called HINT-ATAC (Hmm-based identification of TF footprints using ATAC-seq) and a curated collection of sequence-binding motifs for 809 TFs from CIS-BP (Fig. 3A, step 2) (*25*). By combining peak-gene and TF-peak links, we constructed TF-gene links and generated sample-specific regulatory networks (Fig. 3A, steps 3 and 4). We define TF out-degree as the number of target genes a given TF regulates in the network (fig. S7).

Next, we identified the key TFs for each subtype as those at the top of the gene regulation hierarchy (Fig. 3D and table S8). Each TF is ranked according to a combination of three metrics: (i) its differential out-degree *O_diff* (fig. S8A), (ii) its differential chromatin accessibility at its motifs *A_diff* (fig. S8B), and (iii) its differential gene expression *E_diff* in a given subtype relative to others (Fig. 3D). We assigned ranks to the TFs independently on the basis of the three metrics and added up the three ranks to get the final *TF_rank*.

In CRPC-AR, AR and FOXA1 were the top two TFs, validating our approach (*26*, *27*). In CRPC-NE, the top two TFs were neurogenic differentiation factor 1 (NEUROD1) and achaetescute homolog 1 (ASCL1). NEPC and small-cell lung cancer (SCLC) have been shown to be similar at the phenotypic and molecular level, and ASCL1 and NEUROD1 have been demonstrated to be the main drivers in SCLC (*11*, *28*). In CRPC-WNT, transcription factor 7–like 2 (TCF7L2) was the highest-ranked TF. Also known as TCF-4, TCF7L2 has been shown to be the key driver in colorectal cancer upon upstream Wnt pathway gene alterations such as APC mutations (*29*). Other TCF and lymphoid enhancer binding factor (LEF) TFs were also among the top candidates, including LEF1/LEF, TCF7/TCF-1, and TCF7L1/TCF-3. Upon Wnt pathway activation, β-catenin translocates to the nucleus and coactivates TCF/LEF to promote the expression of downstream genes (*29*).

In CRPC-SCL, we identified the AP-1 family among the top TFs, with FOSL1 having the highest rank. AP-1 is a TF complex assembled through homo- or heterodimerization of members of the Fos and Jun family (*30*). The Fos family includes FOSL1, FOSL2, FOS, and FOSB, whereas the Jun family includes JUN, JUNB, and JUND. AP-1 has been shown to be activated by multiple upstream signals, including growth

Corrected 7 February 2023. See full text.

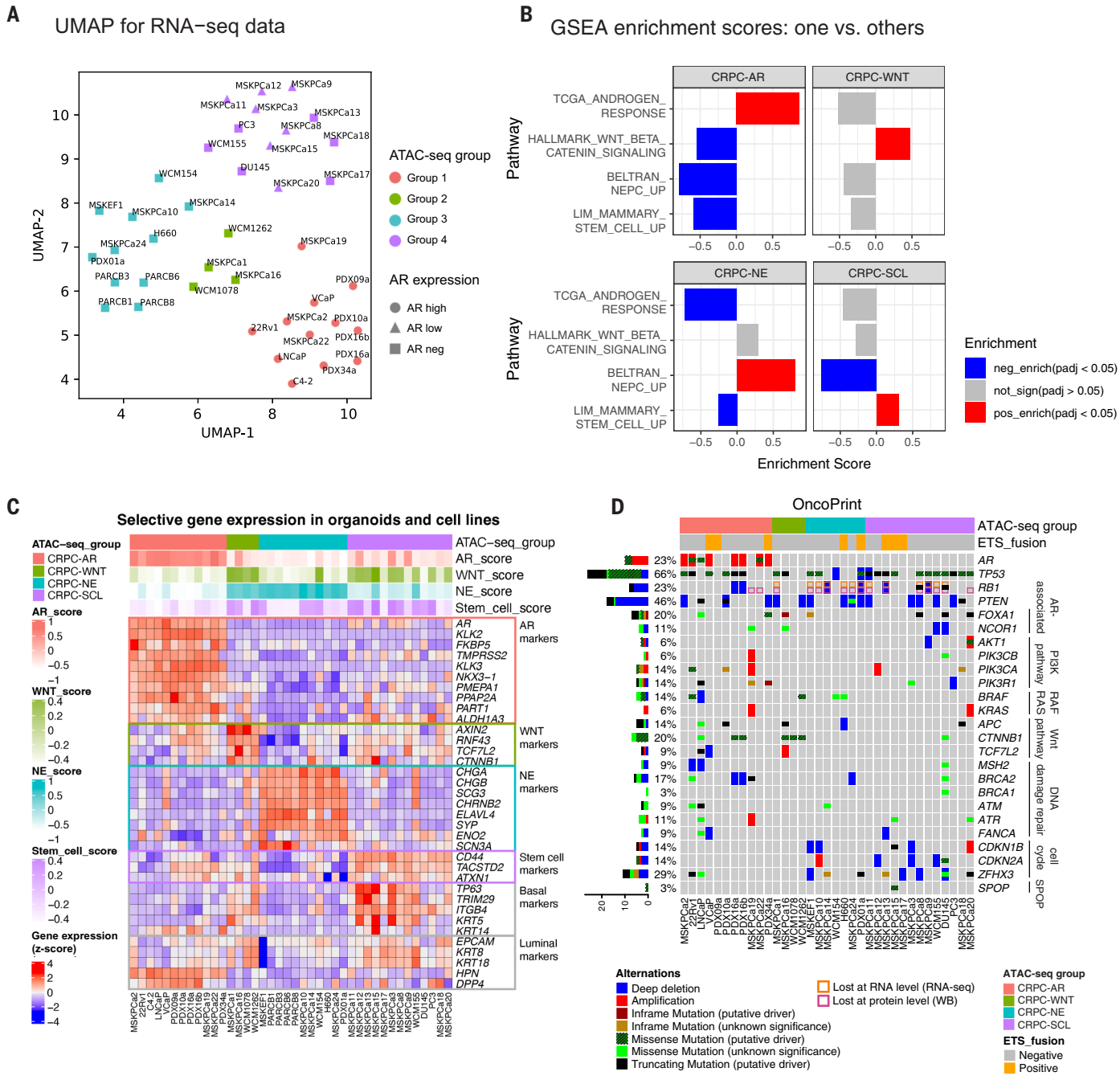

Fig. 2. Transcriptomic and genomic characterization of the four CRPC subtypes defined by ATAC-seq. (**A**) Unsupervised UMAP on the mRNA expression values of the 1000 most variably expressed genes across all samples. (**B**) Enrichment scores and *P* values from GSEA indicate that the four signals are significantly positively enriched in specific subtypes but not in others. (**C**) Heatmap shows the relative expression of subtype-specific marker genes and basal/luminal genes across all samples. The ATAC-seq group and signature scores of the four representative pathways for each sample are shown at the top. (**D**) OncoPrint shows the genomic alterations of the 35 samples with DNA-sequencing data. MSKPCa8 to 20, 22, and 24 were sequenced with MSK-IMPACT. The SNVs and CNVs for cell lines (LNCaP, 22Rv1, VCaP, H660, DU145, and PC3) were collected from CCLE (Cancer Cell Line Encyclopedia). Whole-exome sequencing (WES) was performed for other samples.

factors, hormones, cytokines, inflammation, and stresses. It controls the expression of many downstream genes related to cell division, apoptosis, cell migration, and immunity (*30*).

In addition to subtype-specific TF identification, we also predicted the important TFs in a sample-specific manner. To do this, we analyzed all TFs' relative expression and chromatin accessibility at their motifs for samples in CRPC-WNT, CRPC-NE, and CRPC-SCL, and compared these to the average for CRPC-AR samples. This analysis demonstrated that the key TFs identified in a subtype-specific manner agree with the sample-specific results (fig. S9). We also found significant correlation between the expression of key TFs and accessibility at their motifs, which suggests that they likely exhibit pioneering activity (fig. S10,

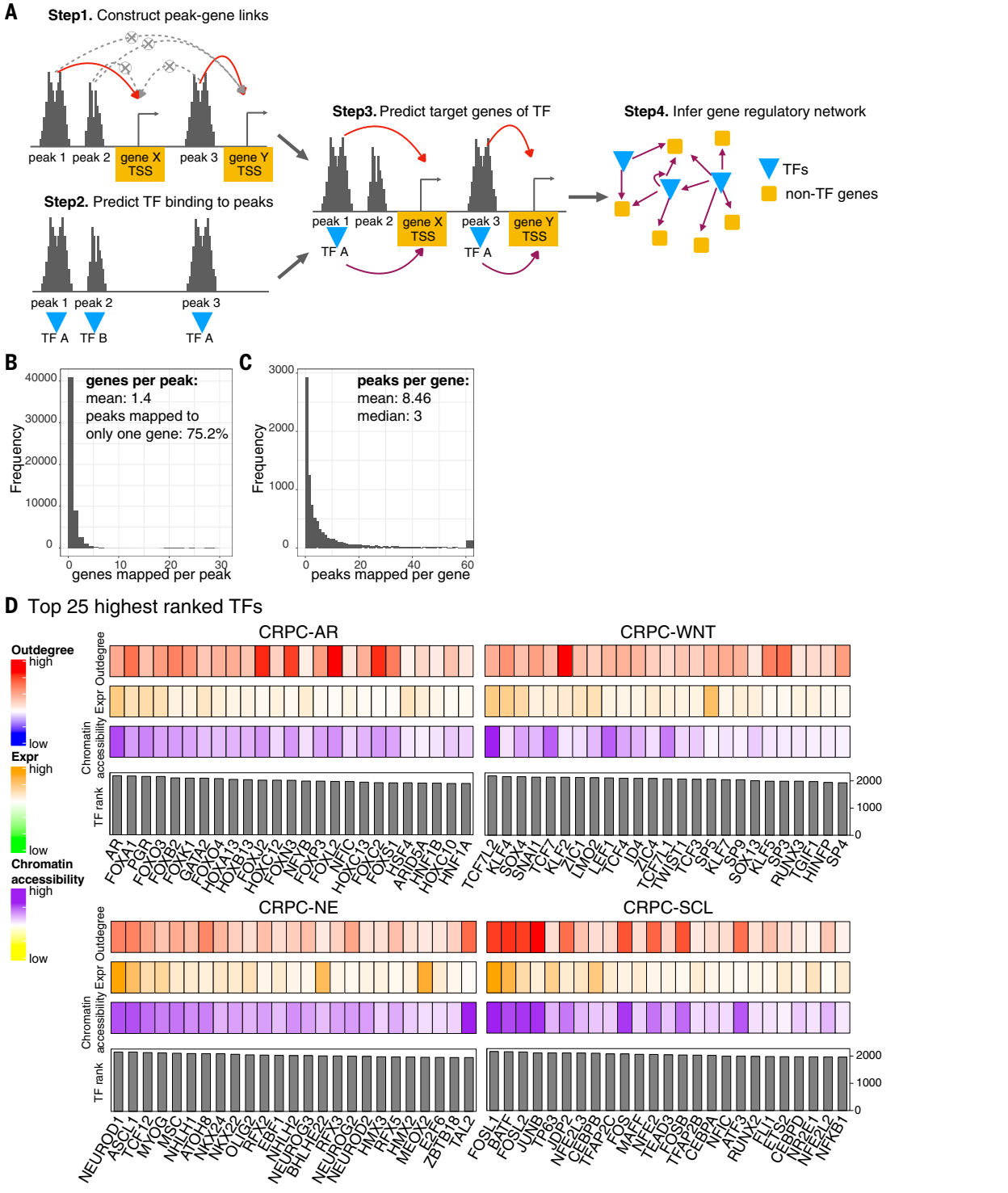

Fig. 3. Identification of the key transcription factors (TFs) of each subtype. (**A**) Schematic illustrating the construction of sample-specific regulatory networks using ATAC-seq and RNA-seq data. (**B**) Distribution of the number of genes linked per peak. (**C**) Distribution of the number of peaks linked per gene. (**D**) Rank order of the top 25 TFs for each of the four subtypes. For each TF, the relative contributions of three metrics to TF rank are shown (Expr, expression). In CRPC-SCL, FOSL1, BATF, FOSL1, JUNB, JDP2, FOS, MAFF, FOSB, and ATF3 belong to the AP-1 family.

adjusted $P < 0.05$) (*12*). Finally, the relative expression levels of predicted key TFs in each of the four groups were confirmed by a quantitative polymerase chain reaction (qPCR) (fig. S3C).

Classification of CRPC patients using transcriptomic signatures of the four subtypes

Next, we examined RNA-seq datasets from 366 CRPC patients to assign each patient to the four subtypes (*21*). We derived the signature genes for each of the four subtypes as the ones with higher expression in one group relative to others in organoids and cell lines, and filtered out genes with low expression or low variance in CRPC patient samples

Corrected 7 February 2023. See full text.

(tables S5 and S9). A template was constructed for each subtype by combining the top signature genes. To assign the CRPC patient samples to a subtype, we used the nearest template prediction (NTP) algorithm (*31*, *32*), which involves computing the cosine distance (*d*) between each patient's RNA-seq data and each of the four templates and estimating the statistical significance by random resampling (Fig. 4A). We applied the method to two cohorts of CRPC patients with polyA-enriched RNA-seq data, including 266 published SU2C patients (*21*)

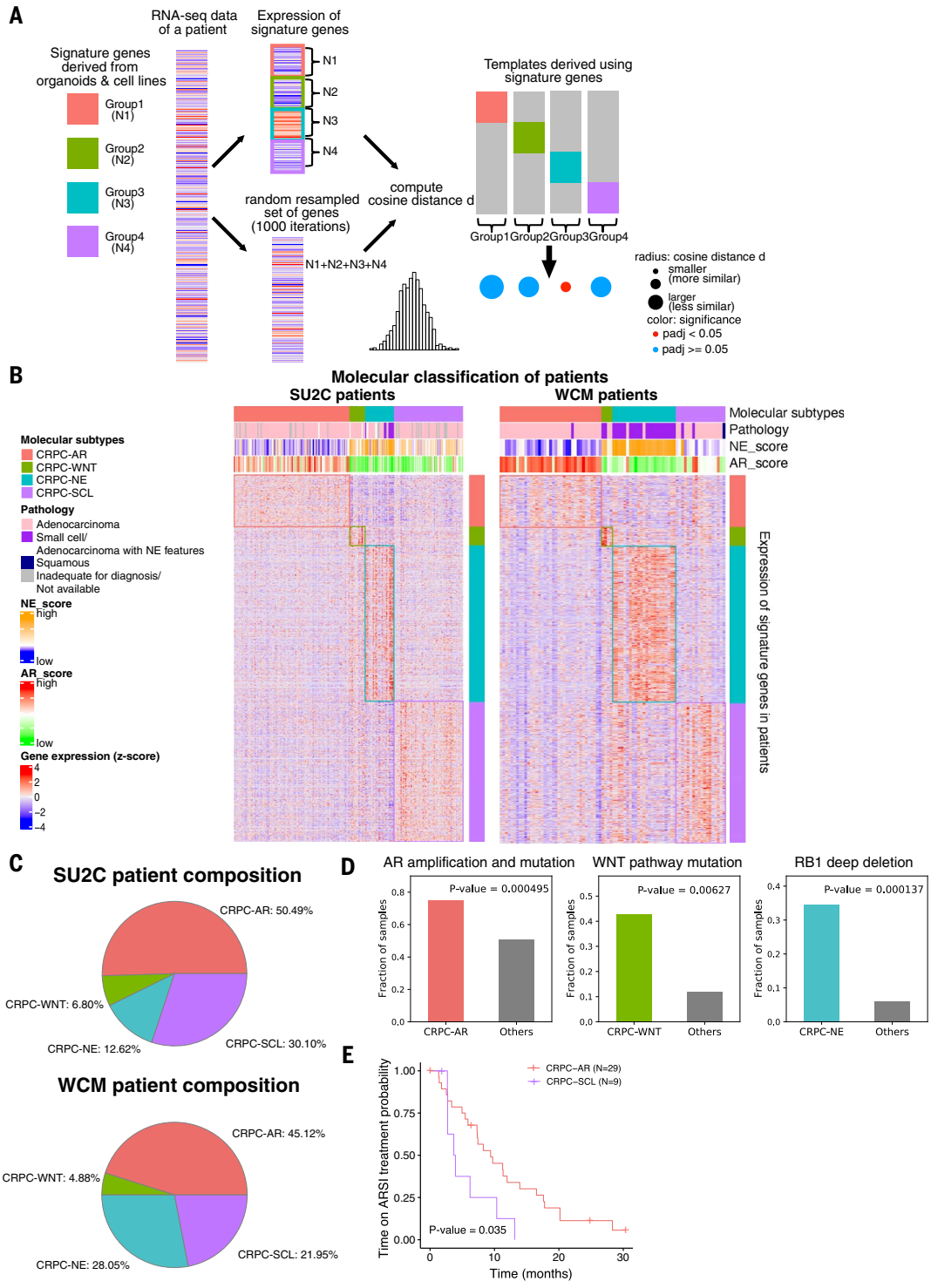

Fig. 4. Classification of CRPC patients using transcriptomic signatures for the four subtypes. (**A**) Schematic illustrating the assignment of each patient to one of the four groups using nearest template prediction. (**B**) Heatmaps showing relative expression of signature genes in SU2C and WCM patients. Top annotations indicate the AR score, NE score, pathology classification, and molecular subtypes of each patient. (**C**) Patient compositions for SU2C and WCM cohorts. (**D**) AR amplification and mutation, WNT pathway component mutations, and RB1 deep deletion are enriched in CRPC-AR, CRPC-WNT, and CRPC-NE SU2C patients, respectively (two-sided Fisher's exact test). (**E**) CRPC-SCL patients exhibit shorter time on ARSI treatment relative to CRPC-AR SU2C patients.

and 100 patients sequenced at Weill Cornell Medicine (WCM) (Fig. 4B). The majority of the patients (206 of 266 SU2C, 82 of 100 WCM) were assigned to one of the four subtypes (table S10). The relative ratios of the four subtypes of patients were similar between cohorts, with the largest group being CRPC-AR, then CRPC-SCL or CRPC-NE, and finally CRPC-WNT as the smallest (Fig. 4C). For WCM1078, WCM1262, WCM155, and MSKPCa2 organoids, RNA-seq data were available from matching tumor samples, which were assigned to the same subtype as the organoids (table S10).

As a complementary approach, we developed a linear SVM (support vector machine) using the gene expression data of the signature genes. Patients were assigned to the four subtypes on the basis of the highest probability from SVC (C-support vector classification). Application of the model to patients' RNA-seq data showed that for most subtypes, the mean probability of patient assignment to that subtype was ≥0.50 (table S10), indicating confident assignment to one group. The majority of samples were assigned the same subtype with either NTP or SVM (92% of WCM and 85% of SU2C samples). The samples unassigned by NTP tended to show more heterogeneity based on SVM (lower highest probabilities compared to the assigned, $P = 4.36 \times 10^{-6}$ for WCM and 1.73×10^{-6} for SU2C, Wilcoxon rank-sum test) and a tendency toward CRPC-SCL ($P = 0.033$ for WCM and 0.00029 for SU2C, Fisher's exact test), potentially pointing to transition to/via this subtype.

The genomic alterations, marker gene expression, and pathologic analysis provided validation of patient classification. CRPC-AR patients showed enrichment of *AR* amplification (Fig. 4D and fig. S11A) and had higher *AR* expression and AR score (Fig. 4B and fig. S11, B and C) compared to other groups. CRPC-NE patients had higher *SYP* expression and NE score (*21*) (fig. S11, B and C) compared to others, and their genotypes were enriched with *RB1* deep deletion (Fig. 4D and fig. S11A). The majority of patients in this class were also diagnosed as having either small-cell, NEPC, or adenocarcinoma with NE features on the basis of histology analysis (Fig. 4B). Patients in CRPC-WNT showed elevated expression of *AXIN2* (fig. S11B) and an enrichment of mutations of Wnt pathway components (Fig. 4D and figs. S11A and S12A). We observed increased expression of the stem cell marker *CD44* in CRPC-SCL patients (fig. S11B) compared to others, as expected, but no consistent enrichment of gene or pathway alterations at the genomic level (figs. S11A and S12B). Moreover, consistent with the results in the 40 models, we found an enrichment of basal signature in the three AR-low/negative groups relative to CRPC-AR (fig. S12C).

Among the 266 SU2C patients, 56 had time-on-treatment data for the next-generation ARSIs enzalutamide and abiraterone acetate. We found that patients classified as CRPC-SCL exhibited shorter time on ARSI treatment using Cox log-rank statistics (Fig. 4E), indicating that the ARSI treatments were less effective for CRPC-SCL patients. We could not compare the time on ARSI treatment for CRPC-AR or CRPC-SCL to other subtypes because there were fewer than five samples for CRPC-WNT and CRPC-NE (table S11).

AP-1 cooperates with YAP, TAZ, and TEAD in CRPC-SCL

The proportion of patients classified as CRPC-SCL was the second largest in the combined SU2C and WCM cohorts (28%) (Fig. 4C and table S10); thus, we further explored samples in this subtype. We focused on MSKPCa3, an AR-low organoid, and DU145, an AR-negative cell line, as CRPC-SCL models for experimental validations.

We identified an AP-1 family member, FOSL1, as the top candidate key TF for CRPC-SCL (Fig. 3D). Expression of various AP-1 components across the four subtypes confirmed *FOSL1* as the AP-1 gene with highest relative expression in CRPC-SCL samples compared to others (fig. S13A), whereas it was barely detectable in CRPC-AR samples at mRNA and protein levels (fig. S13, A and B). To directly assess the importance of FOSL1 for tumor growth, we performed cell competition assays in MSKPCa3 and DU145, with CRPC-AR organoid MSKPCa2 as a control. We transduced the cells with constructs containing green fluorescent protein (GFP), Cas9, and single guide RNAs (sgRNAs) against *FOSL1*, *RPA3* (positive control), or *Rosa26* (negative control) and monitored the relative proportion of GFP-positive sgRNA-expressing cells over time by fluorescence-activated cell sorting (FACS) (fig. S13C). Depletion of GFP-positive sg*FOSL1* was observed in both MSKPCa3 and DU145, but not in MSKPCa2, supporting our prediction that FOSL1 is important for tumor progression in CRPC-SCL (Fig. 5A and fig. S13, D and E).

TFs work together and bind cooperatively in a context-specific manner to achieve specificity and execute their functions (*33*). Thus, to further investigate the regulation of CRPC-SCL samples by AP-1, we investigated the other top TFs identified from chromatin accessibility profiles. We found that TEAD motifs were the second most enriched after AP-1 in the CRPC-SCL–specific accessible peaks (fig. S14A) and they ranked highly on the basis of the gain of chromatin accessibility and out-degree in CRPC-SCL samples (fig. S14B). TEAD TFs are activated by YAP and TAZ transcriptional coactivators (*34*). In fact, motif analysis of the chromatin immunoprecipitation sequencing (ChIP-seq) peaks of YAP and TAZ has revealed that TEAD TFs are the main platform by which these proteins interact with DNA (*34*). TEAD, YAP, and TAZ were reported to be associated with AP-1 genome-wide to jointly regulate the proliferation and motility in multiple cancers, including breast, colorectal, and lung (*35*). In addition, *TAZ* (*WWTR1*) is among the top genes codependent with *FOSL1* based on CRISPR (Avana) Public 20Q2 in DepMap (*36*) with a Pearson correlation of 0.33, further supporting the model in which FOSL1 functions together with YAP and TAZ. From ATAC-seq data and published literature, we hypothesized that YAP, TAZ, TEAD, and AP-1 (FOSL1) may function together to promote the oncogenic growth of CRPC-SCL tumors (Fig. 5B). This is supported by our observation that GSEA using the combined YAP and TAZ (YAP/TAZ) target signature as defined in (*37*) revealed strong enrichment [false discovery rate (FDR) < 0.001] in CRPC-SCL compared to other samples (Fig. 5C). CRPC-SCL also showed significantly higher expression of *YAP* and *TAZ* (fig. S14C; $P < 0.05$, Wilcoxon rank-sum test), and qPCR analysis of representative YAP/TAZ target genes across the 28 samples showed their high expression in this group (fig. S14D).

To validate the co-binding of AP-1 (FOSL1), TEAD, YAP, and TAZ, we performed ChIP-seq in MSKPCa3 and DU145. We found significant enrichment of overlaps between the ChIP-seq peaks of these proteins in both MSKPCa3 and DU145, pointing to their cooperation (Fig. 5, D and E, fig. S15, A and B, and table S12; $P < 0.001$, Fisher's exact test). We also found significant overlap between the target genes of AP-1 and TEAD predicted in our regulatory networks (fig. S15C; $P < 0.001$, Fisher's exact test).

We found that the ChIP-seq peaks of all these four proteins exhibit large overlap with CRPC-SCL ATAC-seq peaks, but barely any with CRPC-AR peaks (Fig. 5F and figs. S15D and S16). Correspondingly, we also observed a strong enrichment of the ChIP-seq signal over CRPC-SCL–specific ATAC-seq peaks relative to the other three subtypes (Fig. 5F and fig. S16; $P < 0.0001$, one-sided Fisher's exact test). As a negative control, the trend was opposite for AR ChIP-seq peaks, in which they showed much larger overlap and signal enrichment at CRPC-AR peaks compared to CRPC-SCL, as expected (Fig. 5F and fig. S16; $P < 0.0001$, one-sided Fisher's exact test) (*38*, *39*). For example, the ChIP-seq and ATAC-seq profiles illustrated open chromatin and binding of AP-1, YAP, TAZ, and TEAD at enhancers of the representative YAP/TAZ target genes, *CYR61* and *AXL*, in CRPC-SCL lines; the same loci were barely accessible in other groups (figs. S17 and S18).

To determine the role of YAP and TAZ in growth, we used small interfering RNA (siRNA) to knock down *YAP* and *TAZ* alone or together in MSKPCa3 and DU145 cells (Fig. 6, A and B, and fig. S19, A and B; $P < 0.05$, two-tailed unpaired *t* test). We observed a significant decrease of cell growth upon *TAZ* and *YAP*/*TAZ* double knockdown in both MSKPCa3 and DU145 but not in the AR-dependent lines MSKPCa2

Corrected 7 February 2023. See full text.

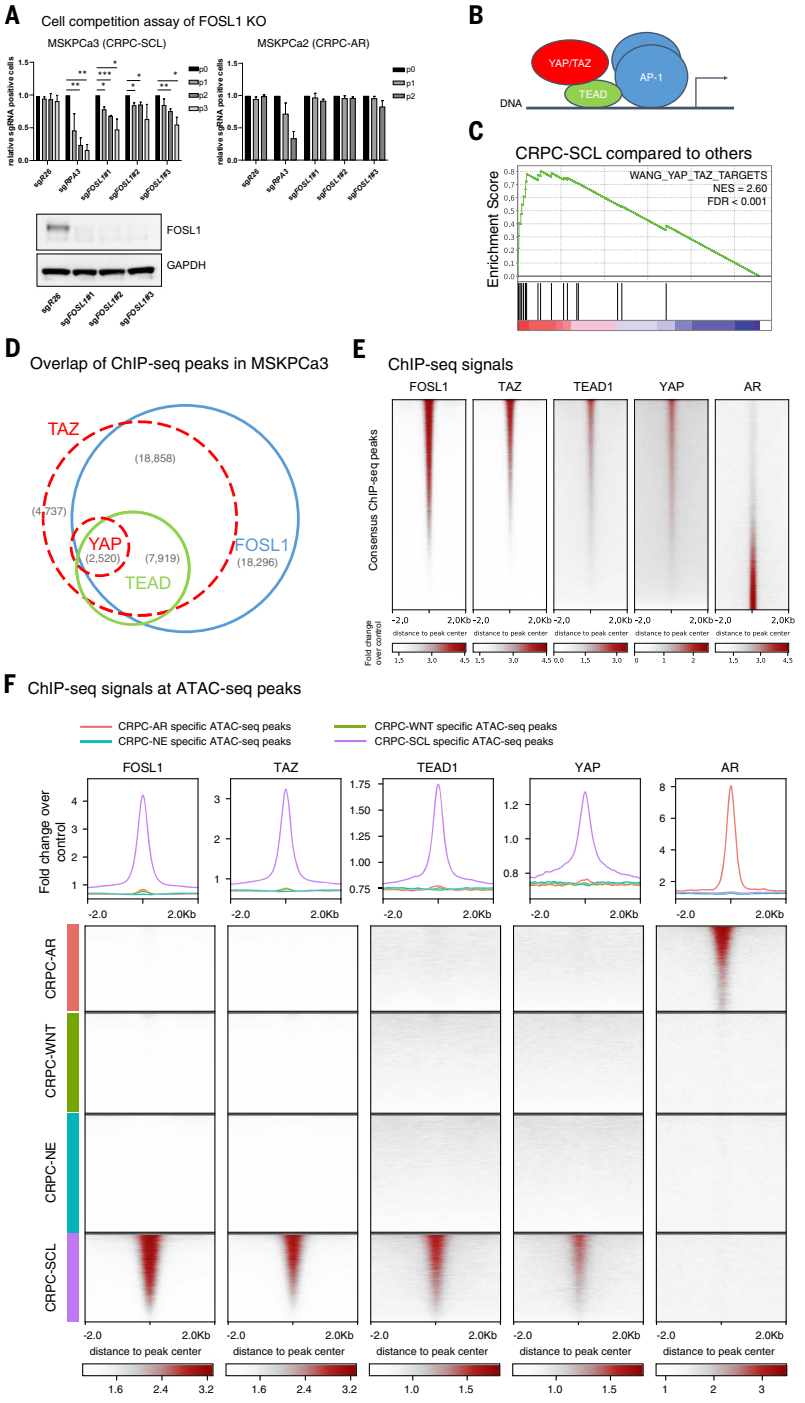

Fig. 5. AP-1 works together with YAP, TAZ, and TEAD in CRPC-SCL. (**A**) Percentage of GFP-positive MSKPCa3 (left) or MSKPCa2 (right) expressing CRISPR guides against FOSL1 or sgR26 (negative control) or sgRPA3 (positive control). Mean ± SEM, n = 2 for MSKPCa3, n = 2 for MSKPCa2. ***P < 0.001, **P < 0.01, *P < 0.05 [multiple unpaired t test comparing between passages (p1 versus p0, p2 versus p0, p3 versus p0)]. Knockout of FOSL1 was confirmed in MSKPCa3 by Western blot. (**B**) Schematic showing the cooperation of AP-1 with YAP/TAZ and TEAD in CRPC-SCL samples. (**C**) GSEA plot showing enrichment of YAP/TAZ signature in CRPC-SCL organoids and cell lines compared to other samples. (**D**) Venn diagram showing the overlaps of FOSL1, TEAD, YAP, and TAZ ChIP-seq peaks in MSKPCa3. Overlaps with more than 1000 peaks are marked, and those between YAP/FOSL1 (48 peaks) and YAP/FOSL1/TEAD (4 peaks) are not shown. (**E**) ChIP-seq signal of FOSL1, TAZ, TEAD1, and YAP in MSKPCa3, and AR (GSE61852) from LNCaP on the consensus peak set. (**F**) ChIP-seq signal of FOSL1, TAZ, TEAD1, and YAP in MSKPCa3, and AR (GSE61852) from LNCaP on subtype-specific ATAC-seq peaks. FOSL1, TEAD1, YAP, and TAZ ChIP-seq peaks for MSKPCa3 show stronger signal at CRPC-SCL–specific ATAC-seq peaks, whereas AR (GSE61852) ChIP-seq peaks have stronger signal in CRPC-AR–specific peaks.

and 22Rv1 (Fig. 6C and fig. S19C; P < 0.0001, two-tailed unpaired t test).

AP-1 and YAP/TAZ are important for subtype-specific chromatin accessibility and gene expression in CRPC-SCL and can be targeted by drugs

Knockdown of FOSL1 and YAP/TAZ shows impact on chromatin accessibility and gene expression

We performed ATAC-seq and RNA-seq in MSKPCa3 cells with knockdown of *FOSL1*, *YAP*, *TAZ*, and *YAP*/*TAZ* together. We observed a significant decrease of chromatin accessibility at the CRPC-SCL–specific open chromatin sites as well as at regions bound by FOSL1, TEAD, YAP, and TAZ from ChIP-seq upon *FOSL1*, *YAP*, and *YAP*/*TAZ* knockdown (Fig. 6, D and E, and fig. S20) (P < 0.001, permutation test). The signal was strongest upon *FOSL1* and double *YAP*/*TAZ* knockdown and highlights their important role in maintaining the chromatin accessibility landscape for the CRPC-SCL group. In agreement with the decrease in chromatin accessibility, we found that CRPC-SCL peaks are the most enriched among down-regulated ATAC-seq peaks upon *FOSL1*, *YAP*, and *YAP*/*TAZ* knockdown (table S13). Moreover, we found that the TEAD and AP-1 motifs are the most enriched at the regions where chromatin accessibility is reduced upon *YAP*/*TAZ* double knockdown, further confirming the model in which YAP and TAZ cooperate with AP-1 and TEAD (fig. S21A). Consistent with ATAC-seq results, we found down-regulation of YAP/TAZ targets in RNA-seq data in all knockdown assays (Fig. 6F and fig. S21B). Double knockdown of *YAP* and *TAZ* showed stronger inhibition of canonical downstream targets (*CTGF*, *CYR61*, *AJUBA*, and *ANKRD1*) and cell cycle–regulating gene *CCND1* (Fig. 6A and fig. S19A), which have been reported as YAP/TAZ targets in various model systems, relative to individual knockdown of *YAP* or *TAZ* (*35*, *40*). Although we also observed enrichment of CRPC-SCL genes among the down-regulated genes, their enrichment in the up-regulated gene set showed that ATAC-seq changes are likely a more meaningful marker to analyze lineage plasticity, as also demonstrated by previous studies (table S14) (*41*). Similar chromatin accessibility and gene expression changes were observed upon *YAP*, *TAZ*, and *YAP*/*TAZ* knockdown in DU145 (figs. S21, C and D, and S22).

Positive feedback loop between YAP/TAZ and FOSL1

We found that *YAP*/*TAZ* double knockdown caused robust depletion of FOSL1, the predicted master TF, at RNA and protein levels in both MSKPCa3 and DU145 (Fig. 6, A and B, and fig. S19, A and B). Moreover, in our regulatory networks for CRPC-SCL samples, *FOSL1* was predicted to be a target of FOS/JUN itself as

Corrected 7 February 2023. See full text.

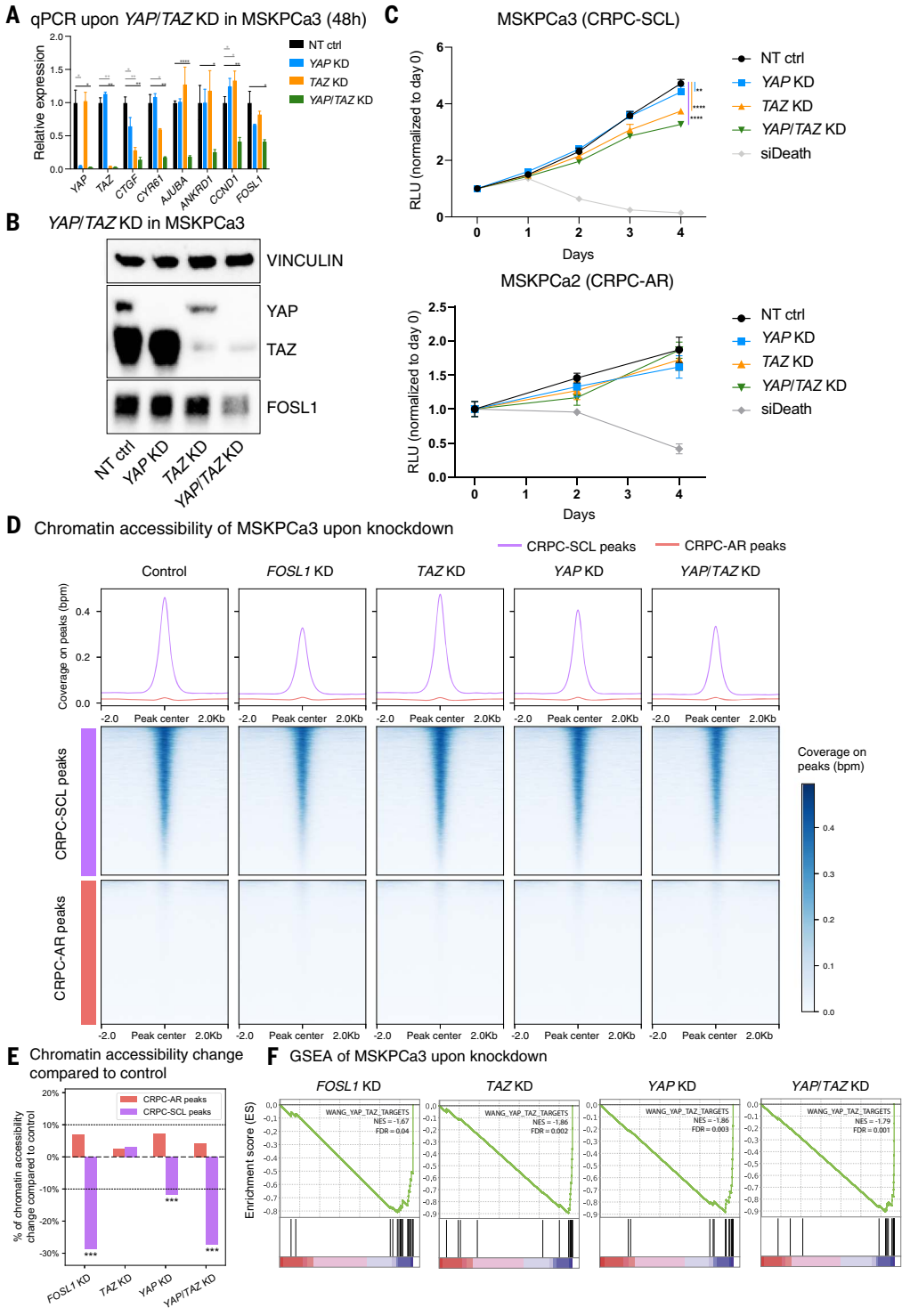

Fig. 6. Impact of *FOSL1*, *YAP*, *TAZ*, and *YAP/TAZ* knockdown. (**A**) qPCR showing that double knockdown of *YAP/TAZ* by siRNA in MSKPCa3 leads to decreased expression of downstream target genes and *FOSL1*. Mean ± SD, $n = 3$. Nontargeting (NT) siRNA serves as the negative control. $^{****}P < 0.0001$, $^{**}P < 0.01$, $^{*}P < 0.05$ (two-tailed unpaired t test); KD, knockdown. (**B**) Western blot (WB) confirming the knockdown efficiency and the decrease of FOSL1 expression 72 hours after transfection in MSKPCa3. (**C**) Cell growth curves of MSKPCa3 and MSKPCa2 after siRNA knockdown. Mean ± SD, $n = 8$ for MSKPCa3, $n = 4$ for MSKPCa2. $^{****}P < 0.0001$, $^{**}P < 0.01$ (two-tailed unpaired t test). (**D**) Chromatin accessibility changes upon *FOSL1*, *TAZ*, *YAP*, and *YAP/TAZ* knockdown at CRPC-AR and CRPC-SCL peaks. (**E**) Average percentage of chromatin accessibility changes upon *FOSL1*, *TAZ*, *YAP*, and *YAP/TAZ* knockdown compared to control at CRPC-AR and CRPC-SCL peaks. $^{***}P < 0.001$ (permutation test). (**F**) GSEA plots showing negative enrichment of YAP/TAZ target genes in MSKPCa3 upon knockdown of *FOSL1*, *TAZ*, *YAP*, and *YAP/TAZ*.

well as TEAD, which cooperates with FOSL1 in our proposed model, similar to observations in other cancers (*35*). Using ChIP-seq data, we also found that the CRPC-SCL–specific *FOSL1* enhancer is bound by TEAD, YAP, TAZ, and FOSL1 (fig. S23). Together, the results suggest that YAP, TAZ, TEAD, and FOSL1 increase the expression of *FOSL1* itself, forming a positive feedback loop to further open chromatin (fig. S24A).

Exogenous expression of FOSL1 alters chromatin accessibility and gene expression from CRPC-AR toward CRPC-SCL

To determine whether FOSL1 could alter the chromatin accessibility landscape and activate the CRPC-SCL signature, we stably expressed *FOSL1* alone or in combination with *YAP* or *TAZ* in LNCaP cells. We observed an increase in chromatin accessibility at CRPC-SCL–specific open chromatin sites in all assays with exogenous expression of *FOSL1*, providing evidence of its role as a pioneering factor in potential lineage plasticity (Fig. 7, A and B; $P < 0.001$, permutation test). We also observed a decrease in chromatin accessibility at CRPC-AR–specific open chromatin sites in all *FOSL1* overexpression assays, further pointing toward lineage transformation (Fig. 7, A and B; $P < 0.001$, permutation test). The RNA-seq results were consistent with ATAC-seq results, and we observed significant up-regulation of CRPC-SCL signature genes with *FOSL1* overexpression, either alone or with *YAP* or *TAZ* (Fig. 7C and fig. S24B, FDR < 10^{-5}).

Small-molecule inhibitors for CRPC-SCL

We used two small-molecule inhibitors that act on the YAP/TAZ/AP-1 pathway for their potential use as therapeutics for CRPC-SCL tumors. Verteporfin is a benzoporphyrin derivative and a medication used as a photosensitizer approved by the FDA for the treatment of age-related macular degeneration. It has been widely reported to inhibit YAP/TAZ and cellular proliferation of multiple tumors (*42*). Consistent with the role of YAP/TAZ in CRPC-SCL, we found that MSKPCa3 and DU145 cells were more sensitive to verteporfin than were MSKPCa2 and 22Rv1, respectively (Fig. 7D and fig. S24, C and D). T-5224 is a c-Fos/AP-1 inhibitor, specifically affecting the DNA binding activity of c-Fos/c-Jun and under clinical trial for use in other cancers and diseases (*43*). We found that T-5224 inhibited MSKPCa3 and DU145 cell growth in a dose-dependent fashion, whereas it had no effect on MSKPCa2 and 22Rv1 (Fig. 7E and fig. S24, D and E).

The YAP/TAZ pathway is enriched in CRPC-SCL patients

Finally, we examined YAP/TAZ activity in transcriptomic data from CRPC patients from both SU2C and WCM. YAP/TAZ pathway activity (sum of z-scores) was significantly higher in CRPC-SCL patients relative to all samples (Fig. 7F; $P < 0.01$, one-tailed Wilcoxon rank-sum test), with higher expression of *YAP*, *TAZ*, and representative downstream genes (fig. S25A). We also observed a significant negative correlation between *AR* expression and YAP/TAZ pathway activity across all SU2C samples (Fig. 7G and fig. S25B; $P < 0.001$).

Discussion

We used a diverse biobank of organoids and PDXs that recapitulate the genotypic and phenotypic heterogeneity of metastatic prostate cancer to generate a map of the chromatin accessibility and transcriptomic landscape of CRPC. In so doing, we validated the CRPC-AR and CRPC-NE subtypes and identified two subtypes of AR-negative/low samples. Our integrated use of ATAC-seq and RNA-seq data allowed us to identify the master TFs driving AR-negative/low CRPCs. Previous studies using only RNA-seq data could not identify these drivers because GSEA identifies numerous biological processes that are enriched among CRPC-SCL samples (fig. S4A), complicating efforts to find driver events. Furthermore, our work shows that CRPC-SCL constitutes the second most prevalent group of CRPC patients, exhibits lower AR expression and AR transcriptional output, and is associated with shorter time under ARSI treatment compared to CRPC-AR.

Integrated analysis of ATAC-seq, RNA-seq, and ChIP-seq data revealed a model in which YAP, TAZ, TEAD, and AP-1 function together and drive oncogenic growth in CRPC-SCL samples. We validated this with CRISPR and depletion studies using siRNA knockdown. From overexpression assays in AR-high LNCaP cells, we showed how FOSL1 functions as a pioneering factor and master regulator for CRPC-SCL. This model reveals potential therapeutic vulnerabilities in CRPC-SCL tumors by inhibition of the YAP/TAZ/AP-1 pathway.

Prior studies support these conclusions. For example, the Wnt pathway has been identified as a driver of metastasis and resistance to AR-targeted therapies (*44*, *45*). Furthermore, knocking down *TAZ* in DU145 (CRPC-SCL from our study) decreased cell migration and metastasis, whereas overexpression of *TAZ* in RWPE (normal prostate cells) promoted cell migration, epithelial-mesenchymal transition, and anchorage-independent growth (*46*). Overexpression of *YAP* has been reported to promote cell proliferation, invasion, and castration-resistant growth in LNCaP and RWPE (*47*). In addition, YAP/TAZ activation has been found to be related to cell proliferation, therapy resistance, and metastasis in various other tumor types by extensive rewiring of the epigenome of differentiated cells, reprogramming them into stem-like cells and conferring lineage plasticity (*34*, *35*). These lines of evidence along with those from our study show the importance of AP-1, YAP, and TAZ in the generation and maintenance of the chromatin and transcriptomic landscape in a specific subtype of CRPC.

Enrichment of basal signature, such as we saw in CRPC-SCL organoids and patient samples, has been observed in prostate cancer cell lines after depletion of TP53 and RB1 (*16*, *19*) and is also observed in models of DNPC derived from AR knockout of luminal prostate cancer cells (*5*). This suggests that CRPC-SCL tumors acquire lineage plasticity similar to NEPC but are driven by different master TFs, resulting in a different phenotype. Because CRPC-SCL tumors are pathologically adenocarcinoma without neuroendocrine features, our study may guide the use of ARSIs in these cases. However, this requires further detailed mechanistic studies of lineage transformation and heterogeneity among the four subtypes. Moreover, future in vivo studies over longer time periods are needed to provide further insights about the efficacy and specificity of small molecules that target this subtype. Although we showed the differential impact of verteporfin on CRPC-SCL versus CRPC-AR samples, its YAP-independent effects may limit its clinical potential (*48*, *49*). Meanwhile, other AP-1 inhibitors not tested in this study may show high clinical potential for CRPC-SCL (*50*). Overall, we have shown how an approach to stratify CRPC patients into four subtypes using their transcriptomic signatures can potentially inform appropriate clinical decisions.

Methods summary

ATAC-seq and RNA-seq data were generated for 35 metastatic prostate cancer models, including 22 organoids, six PDXs, and seven cell lines. Together with five more derived CRPC cell lines from Park *et al.* (*11*), we uniformly processed ATAC-seq and RNA-seq data from 40 models. The ATAC-seq data were used to cluster the samples and revealed four subtypes. We generated gene signatures of the four epigenetically defined subgroups using RNA-seq data. These gene signatures were used to classify 366 CRPC patient samples. Moreover, we constructed regulatory networks for the models using a correlation-based method connecting ATAC-seq peaks to gene expression and a footprint-based method for TF to regulatory element connections. Key TFs for each subgroup were identified using a metric integrating regulatory network, ATAC-seq, and RNA-seq features. The proposed cooperation between key TFs and other proteins was validated using ChIP-seq. The impact of FOSL1, YAP, and TAZ on subtype-specific chromatin accessibility and gene expression

Corrected 7 February 2023. See full text.

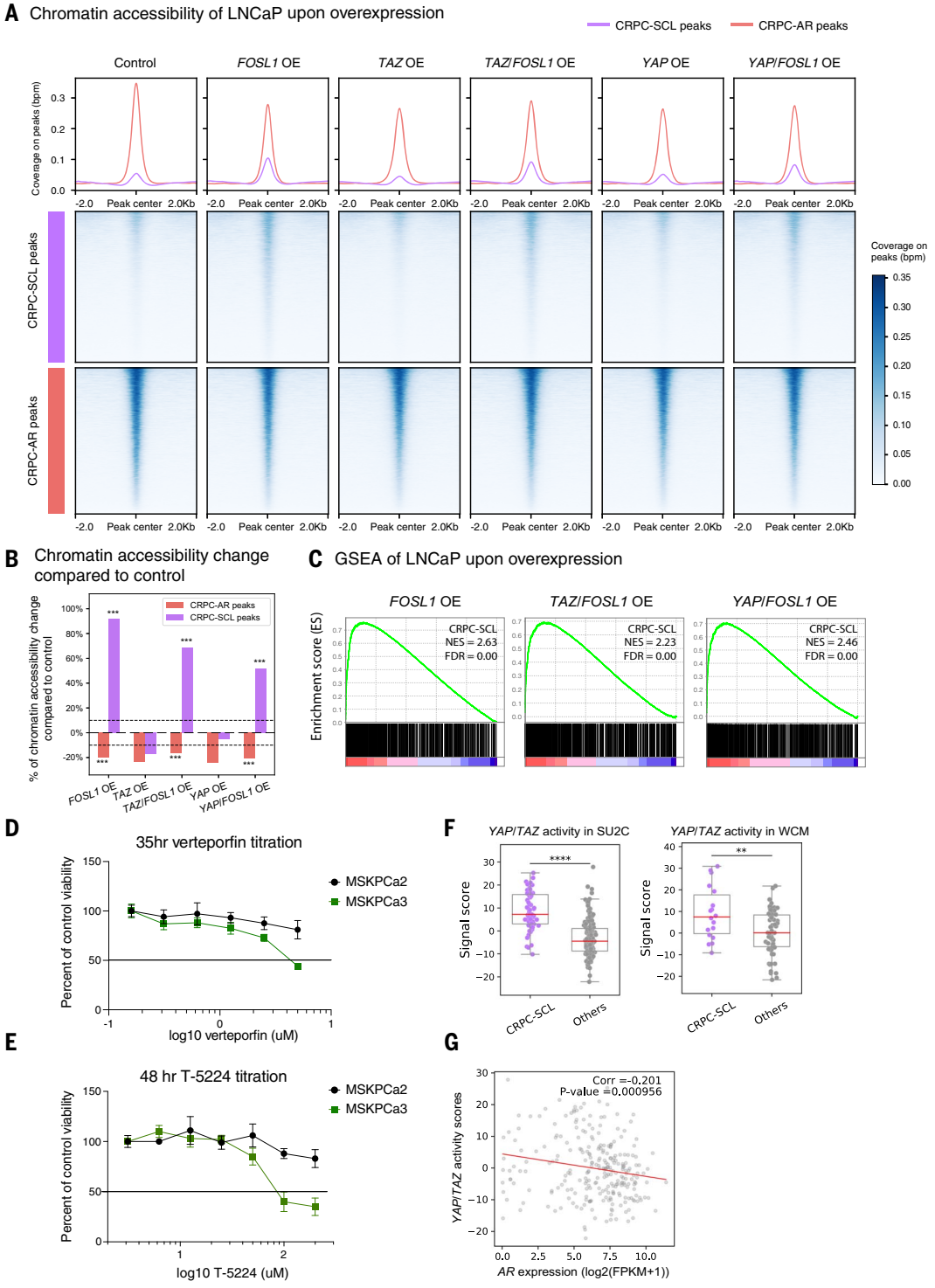

Fig. 7. Evidence of the role of AP-1, YAP, and TAZ in CRPC-SCL from overexpression, small-molecule inhibition, and patient transcriptome findings. (**A**) Chromatin accessibility changes upon *FOSL1*, *TAZ/FOSL1*, *TAZ*, *YAP/FOSL1*, and *YAP* overexpression in LNCaP cells at CRPC-AR and CRPC-SCL peaks. (**B**) Average percentage of chromatin accessibility changes upon *FOSL1*, *TAZ/FOSL1*, *TAZ*, *YAP/FOSL1*, and *YAP* overexpression in LNCaP compared to control at CRPC-AR and CRPC-SCL peaks. ***$P < 0.001$ (permutation test). (**C**) Overexpression of *FOSL1* in LNCaP cells shows up-regulation of CRPC-SCL signature genes. (**D**) Effect of verteporfin on MSKPCa2 (CRPC-AR) and MSKPCa3 (CRPC-SCL) cell growth. (**E**) Effect of T-5224 on MSKPCa2 and MSKPCa3 cell growth. (**F**) YAP/TAZ activity (sum of z-scores) is significantly higher in CRPC-SCL patients. ****$P < 0.0001$, **$P < 0.01$ (one-tailed Wilcoxon rank-sum test, CRPC-SCL compared to the other groups). (**G**) YAP/TAZ activity is negatively correlated with *AR* expression across the 266 SU2C patients with Corr = −0.201 and $P < 0.001$.

of the CRPC-SCL group was validated by knockdown and exogenous overexpression assays followed by ATAC-seq, RNA-seq, and qPCR. Lastly, we tested the effect of two compounds on proliferation and downstream gene expression in both organoids and cell lines.

REFERENCES AND NOTES

1. P. A. Watson, V. K. Arora, C. L. Sawyers, Emerging mechanisms of resistance to androgen receptor inhibitors in prostate cancer. *Nat. Rev. Cancer* **15**, 701–711 (2015). doi: 10.1038/nrc4016; pmid: 26563462
2. Á. Quintanal-Villalonga *et al*., Lineage plasticity in cancer: A shared pathway of therapeutic resistance. *Nat. Rev. Clin. Oncol.* **17**, 360–371 (2020). doi: 10.1038/s41571-020-0340-z; pmid: 32152485
3. D. S. Rickman, H. Beltran, F. Demichelis, M. A. Rubin, Biology and evolution of poorly differentiated neuroendocrine tumors. *Nat. Med.* **23**, 1–10 (2017). doi: 10.1038/nm.4341; pmid: 28586335
4. H. Beltran *et al*., The Role of Lineage Plasticity in Prostate Cancer Therapy Resistance. *Clin. Cancer Res.* **25**, 6916–6924 (2019). doi: 10.1158/1078-0432.CCR-19-1423; pmid: 31363002
5. E. G. Bluemn *et al*., Androgen Receptor Pathway-Independent Prostate Cancer Is Sustained through FGF Signaling. *Cancer Cell* **32**, 474–489.e6 (2017). doi: 10.1016/j.ccell.2017.09.003; pmid: 29017058
6. M. P. Labrecque *et al*., Molecular profiling stratifies diverse phenotypes of treatment-refractory metastatic castration-resistant prostate cancer. *J. Clin. Invest.* **129**, 4492–4505 (2019). doi: 10.1172/JCI128212; pmid: 31361600
7. D. Gao *et al*., Organoid cultures derived from patients with advanced prostate cancer. *Cell* **159**, 176–187 (2014). doi: 10.1016/j.cell.2014.08.016; pmid: 25201530
8. L. Puca *et al*., Patient derived organoids to model rare prostate cancer phenotypes. *Nat. Commun.* **9**, 2404 (2018). doi: 10.1038/s41467-018-04495-z; pmid: 29921838
9. W. Abida *et al*., Prospective Genomic Profiling of Prostate Cancer Across Disease States Reveals Germline and Somatic Alterations That May Affect Clinical Decision Making. *JCO Precis. Oncol.* **2017**, 1–16 (2017). doi: 10.1200/PO.17.00029; pmid: 28825054
10. D. Robinson *et al*., Integrative clinical genomics of advanced prostate cancer. *Cell* **161**, 1215–1228 (2015). doi: 10.1016/j.cell.2015.05.001; pmid: 26000489
11. J. W. Park *et al*., Reprogramming normal human epithelial tissues to a common, lethal neuroendocrine cancer lineage. *Science* **362**, 91–95 (2018). doi: 10.1126/science.aat5749; pmid: 30287662
12. M. R. Corces *et al*., The chromatin accessibility landscape of primary human cancers. *Science* **362**, eaav1898 (2018). doi: 10.1126/science.aat5749; pmid: 30287662
13. M. R. Corces *et al*., Lineage-specific and single-cell chromatin accessibility charts human hematopoiesis and leukemia evolution. *Nat. Genet.* **48**, 1193–1203 (2016). doi: 10.1038/ng.3646; pmid: 27526324
14. Cancer Genome Atlas Research Network, The Molecular Taxonomy of Primary Prostate Cancer. *Cell* **163**, 1011–1025 (2015). doi: 10.1016/j.cell.2015.10.025; pmid: 26544944
15. H. Beltran *et al*., Divergent clonal evolution of castration-resistant neuroendocrine prostate cancer. *Nat. Med.* **22**, 298–305 (2016). doi: 10.1038/nm.4045; pmid: 26855148
16. P. Mu *et al*., SOX2 promotes lineage plasticity and antiandrogen resistance in TP53- and RB1-deficient prostate cancer. *Science* **355**, 84–88 (2017). doi: 10.1126/science.aah4307; pmid: 28059768
17. B. A. Smith *et al*., A basal stem cell signature identifies aggressive prostate cancer phenotypes. *Proc. Natl. Acad. Sci. U.S.A.* **112**, E6544–E6552 (2015). doi: 10.1073/pnas.1518007112; pmid: 26460041
18. V. Murillo-Garzón, R. Kypta, WNT signalling in prostate cancer. *Nat. Rev. Urol.* **14**, 683–696 (2017). doi: 10.1038/nrurol.2017.144; pmid: 28895566
19. S. Y. Ku *et al*., Rb1 and Trp53 cooperate to suppress prostate cancer lineage plasticity, metastasis, and antiandrogen resistance. *Science* **355**, 78–83 (2017). doi: 10.1126/science.aah4199; pmid: 28059767
20. W. S. Chen *et al*., Genomic Drivers of Poor Prognosis and Enzalutamide Resistance in Metastatic Castration-resistant Prostate Cancer. *Eur. Urol.* **76**, 562–571 (2019). doi: 10.1016/j.eururo.2019.03.020; pmid: 30928160
21. W. Abida *et al*., Genomic correlates of clinical outcome in advanced prostate cancer. *Proc. Natl. Acad. Sci. U.S.A.* **116**, 11428–11436 (2019). doi: 10.1073/pnas.1902651116; pmid: 31061129
22. M. D. Nyquist *et al*., Combined TP53 and RB1 Loss Promotes Prostate Cancer Resistance to a Spectrum of Therapeutics and Confers Vulnerability to Replication Stress. *Cell Rep.* **31**, 107669 (2020). doi: 10.1016/j.celrep.2020.107669; pmid: 32460015
23. P. Dhingra *et al*., Identification of novel prostate cancer drivers using RegNetDriver: A framework for integration of genetic and epigenetic alterations with tissue-specific regulatory network. *Genome Biol.* **18**, 141 (2017). doi: 10.1186/s13059-017-1266-3; pmid: 28750683
24. E. Khurana *et al*., Role of non-coding sequence variants in cancer. *Nat. Rev. Genet.* **17**, 93–108 (2016). doi: 10.1038/nrg.2015.17; pmid: 26781813
25. Z. Li *et al*., Identification of transcription factor binding sites using ATAC-seq. *Genome Biol.* **20**, 45 (2019). doi: 10.1186/s13059-019-1642-2; pmid: 30808370
26. E. J. Adams *et al*., FOXA1 mutations alter pioneering activity, differentiation and prostate cancer phenotypes. *Nature* **571**, 408–412 (2019). doi: 10.1038/s41586-019-1318-9; pmid: 31243370
27. A. Parolia *et al*., Distinct structural classes of activating FOXA1 alterations in advanced prostate cancer. *Nature* **571**, 413–418 (2019). doi: 10.1038/s41586-019-1347-4; pmid: 31243372
28. C. M. Rudin *et al*., Molecular subtypes of small cell lung cancer: A synthesis of human and mouse model data. *Nat. Rev. Cancer* **19**, 289–297 (2019). doi: 10.1038/s41568-019-0133-9; pmid: 30926931
29. H. Clevers, Wnt breakers in colon cancer. *Cancer Cell* **5**, 5–6 (2004). doi: 10.1016/S1535-6108(03)00339-8; pmid: 14749120
30. R. Eferl, E. F. Wagner, AP-1: A double-edged sword in tumorigenesis. *Nat. Rev. Cancer* **3**, 859–868 (2003). doi: 10.1038/nrc1209; pmid: 14668816
31. J. Guinney *et al*., The consensus molecular subtypes of colorectal cancer. *Nat. Med.* **21**, 1350–1356 (2015). doi: 10.1038/nm.3967; pmid: 26457759
32. Y. Hoshida, Nearest template prediction: A single-sample-based flexible class prediction with confidence assessment. *PLOS ONE* **5**, e15543 (2010). doi: 10.1371/journal.pone.0015543; pmid: 21124904
33. S. A. Lambert *et al*., The Human Transcription Factors. *Cell* **172**, 650–665 (2018). doi: 10.1016/j.cell.2018.01.029; pmid: 29425488
34. S. Piccolo, S. Dupont, M. Cordenonsi, The biology of YAP/TAZ: Hippo signaling and beyond. *Physiol. Rev.* **94**, 1287–1312 (2014). doi: 10.1152/physrev.00005.2014; pmid: 25287865
35. F. Zanconato, M. Cordenonsi, S. Piccolo, YAP/TAZ at the Roots of Cancer. *Cancer Cell* **29**, 783–803 (2016). doi: 10.1016/j.ccell.2016.05.005; pmid: 27300434
36. A. Tsherniak *et al*., Defining a Cancer Dependency Map. *Cell* **170**, 564–576.e16 (2017). doi: 10.1016/j.cell.2017.06.010; pmid: 28753430
37. Y. Wang *et al*., Comprehensive Molecular Characterization of the Hippo Signaling Pathway in Cancer. *Cell Rep.* **25**, 1304–1317.e5 (2018). doi: 10.1016/j.celrep.2018.10.001; pmid: 30380420
38. S. Shukla *et al*., Aberrant Activation of a Gastrointestinal Transcriptional Circuit in Prostate Cancer Mediates Castration Resistance. *Cancer Cell* **32**, 792–806.e7 (2017). doi: 10.1016/j.ccell.2017.10.008; pmid: 29153843
39. G. G. Galli *et al*., YAP Drives Growth by Controlling Transcriptional Pause Release from Dynamic Enhancers. *Mol. Cell* **60**, 328–337 (2015). doi: 10.1016/j.molcel.2015.09.001; pmid: 26439301
40. F. Zanconato *et al*., Genome-wide association between YAP/TAZ/TEAD and AP-1 at enhancers drives oncogenic growth. *Nat. Cell Biol.* **17**, 1218–1227 (2015). doi: 10.1038/ncb3216; pmid: 26258633
41. S. Ma *et al*., Chromatin Potential Identified by Shared Single-Cell Profiling of RNA and Chromatin. *Cell* **183**, 1103–1116.e20 (2020). doi: 10.1016/j.cell.2020.09.056; pmid: 33098772
42. F. Gibault *et al*., Molecular Features of the YAP Inhibitor Verteporfin: Synthesis of Hexasubstituted Dipyrrins as Potential Inhibitors of YAP/TAZ, the Downstream Effectors of the Hippo Pathway. *ChemMedChem* **12**, 954–961 (2017). doi: 10.1002/cmdc.201700063; pmid: 28334506
43. Y. Aikawa *et al*., Treatment of arthritis with a selective inhibitor of c-Fos/activator protein-1. *Nat. Biotechnol.* **26**, 817–823 (2008). doi: 10.1038/nbt1412; pmid: 18587386
44. J. Leibold *et al*., Somatic Tissue Engineering in Mouse Models Reveals an Actionable Role for WNT Pathway Alterations in Prostate Cancer Metastasis. *Cancer Discov.* **10**, 1038–1057 (2020). doi: 10.1158/2159-8290.CD-19-1242; pmid: 32376773
45. P. Isaacsson Velho *et al*., Wnt-pathway Activating Mutations Are Associated with Resistance to First-line Abiraterone and Enzalutamide in Castration-resistant Prostate Cancer. *Eur. Urol.* **77**, 14–21 (2020). doi: 10.1016/j.eururo.2019.05.032; pmid: 31176623
46. C.-Y. Liu, T. Yu, Y. Huang, L. Cui, W. Hong, ETS (E26 transformation-specific) up-regulation of the transcriptional co-activator TAZ promotes cell migration and metastasis in prostate cancer. *J. Biol. Chem.* **292**, 9420–9430 (2017). doi: 10.1074/jbc.M117.783787; pmid: 28408625
47. L. Zhang *et al*., The hippo pathway effector YAP regulates motility, invasion, and castration-resistant growth of prostate cancer cells. *Mol. Cell. Biol.* **35**, 1350–1362 (2015). doi: 10.1128/MCB.00102-15; pmid: 25645929
48. H. Zhang *et al*., Tumor-selective proteotoxicity of verteporfin inhibits colon cancer progression independently of YAP1. *Sci. Signal.* **8**, ra98 (2015). doi: 10.1126/scisignal.aac5418; pmid: 26443705
49. V. R. Dasari *et al*., Verteporfin exhibits YAP-independent anti-proliferative and cytotoxic effects in endometrial cancer cells. *Oncotarget* **8**, 28628–28640 (2017). doi: 10.18632/oncotarget.15614; pmid: 28404908
50. N. Ye, Y. Ding, C. Wild, Q. Shen, J. Zhou, Small molecule inhibitors targeting activator protein 1 (AP-1). *J. Med. Chem.* **57**, 6930–6948 (2014). doi: 10.1021/jm5004733; pmid: 24831826

ACKNOWLEDGMENTS

We thank members of the Khurana and Chen laboratories for valuable critiques and discussions; the Genomics Research Core Facility at WCM for ATAC-seq and RNA-seq sequencing; the Englander Institute for Precision Medicine for WCM CRPC patient and organoid data; the Center of Epigenetics Research at MSKCC for ATAC-seq; Integrated Genomics Operation core facility at MSKCC for MSK-IMPACT sequencing; Antitumor Assessment Core Facility at MSKCC for PDX models; and K. Chang at Cold Spring Harbor Laboratory for generously providing LentiV_sgRNA_Cas9_GFP (LgCG) vector and design of sgRNA sequences. F.T. thanks M. A. Rubin (present affiliation: University of Bern, Switzerland) for training in prostate cancer research during her Ph.D. E.K. is an affiliate member of the New York Genome Center. **Funding:** Supported by NIH grants P30CA008748 (Y.C., H.I.S., P.C., A.G., W.A., E.D.S., and M.F.B.), P50CA221745 (Y.C., H.I.S., A.G., W.A., and E.D.S.), P50CA211024 (A.S., E.K., and J.M.M.), R37CA241486 and R37CA241486-02 (H.B.), U54CA224079 (Cancer Moonshot), U01CA224044, R01CA193837, and R01CA208100 (Y.C.), U01CA252048, R01CA228216, and DP2CA174499 (P.C.), R01CA218668 (E.K.); Department of Defense W81XWH-17-1-0653 (H.B.), Prostate Cancer Foundation (Y.C., H.I.S., and W.A.); STARR Cancer Consortium (Y.C., P.C., and H.B.); Geoffrey Beene Cancer Center (Y.C. and P.C.); Irma T. Hirschl Trust (E.K.); and WorldQuant Foundation (E.K.). **Author contributions:** F.T., Y.C., and E.K. conceived of and designed the project. F.T., D.X., C.K.W., Y.C., and E.K. wrote the manuscript with the help of all authors. F.T., S.W., C.J.L., W.D., D.G., W.A., A.G., M.F.B., P.C., H.I.S., and Y.C. performed or supervised the derivation, maintenance, and characterization of the 10 new organoids. F.T., J.P., and C.H. performed sample processing and ATAC-seq library construction. F.T., C.K.W., and S.C. performed functional validation experiments. H.T. constructed shRNA knockdown vectors with supervision from L.E.D. F.T. and D.X. performed the majority of bioinformatic analyses. K.E. performed whole-exome sequencing data analysis for WCM organoids. R.H. provided bam files for WCM patient cohorts' RNA-seq data. E.M.L. assisted with SU2C cohort analysis. A.M.F. assisted with gene expression analysis. A.P. assisted with the collection of organoids and cell lines SNV and CNV data. L.P. and H.B. provided WCM organoids. S.B., L.P., J.M.M., H.B., C.N.S., and A.S. collected and organized the WCM patient information and provided the sequencing data. M.M. and E.D.S. assisted with the PDX models. Y.C. and E.K. supervised the study. **Competing interests:** Y.C. holds interest and receives royalties from ORIC Pharmaceuticals. C.N.S. disclosures: Pfizer, Merck, AstraZeneca, Astellas Pharma, Bayer, Bristol Myers Squibb, Genzyme, Gilead, Incyte, Impact Pharma, Medscape, MSD, Roche, UroToday. L.E.D. is an advisory board member and holds equity in Mirimus Inc. L.E.D. has consulted on gene editing and knockdown technologies for Volastra Therapeutics, Frazier Healthcare, FogPharma, and Revolution Medicines. H.B. has served as consultant/advisory board member for Janssen, Astellas, Astra Zeneca, Merck, Pfizer, Foundation Medicine, Blue Earth Diagnostics, Amgen, Bayer, Oncorus, LOXO, Daiichi Sankyo, and Curie Therapeutics and has received research funding from

Janssen, AbbVie/Stemcentrx, Eli Lilly, Astellas, Millennium, and Bristol Myers Squibb. F.T. is an employee at AbbVie, L.P. is an employee at Loxo Oncology at Lilly, and K.E. is an employee at Illumina. This work was completed prior to their employment in industry. They are acting on their own, and these endeavors are not in any manner affiliated with their current affiliations.
Data and materials availability: RNA-seq data for patients sequenced at WCM are available at EGAS00001006059. ATAC-seq, RNA-seq, and ChIP-seq data from cell lines, PDXs, and organoids are available at Gene Expression Omnibus (GSE199190). MSK-IMPACT mutational states can be found at www.cbioportal.org. Code is available at DOI: 10.5281/zenodo.5885500. New organoid models reported in this work are available from Y.C. under a material transfer agreement with Memorial Sloan Kettering Cancer Center.

SUPPLEMENTARY MATERIALS

science.org/doi/10.1126/science.abe1505
Materials and Methods
Supplementary Text
Figs. S1 to S25
Tables S1 to S17
References (*51*–*79*)
MDAR Reproducibility Checklist

View/request a protocol for this paper from *Bio-protocol*.

Submitted 3 August 2020; resubmitted 18 September 2021
Accepted 20 April 2022
10.1126/science.abe1505

Chromatin profiles classify castration-resistant prostate cancers suggesting therapeutic targets

Fanying Tang, Duo Xu, Shangqian Wang, Chen Khuan Wong, Alexander Martinez-Fundichely, Cindy J. Lee, Sandra Cohen, Jane Park, Corinne E. Hill, Kenneth Eng, Rohan Bareja, Teng Han, Eric Minwei Liu, Ann Palladino, Wei Di, Dong Gao, Wassim Abida, Shaham Beg, Loredana Puca, Maximiliano Meneses, Elisa de Stanchina, Michael F. Berger, Anuradha Gopalan, Lukas E. Dow, Juan Miguel Mosquera, Himisha Beltran, Cora N. Sternberg, Ping Chi, Howard I. Scher, Andrea Sboner, Yu Chen, and Ekta Khurana

Science **376** (6596), eabe1505. DOI: 10.1126/science.abe1505

Grouping prostate cancers

Therapeutic interventions are needed for prostate tumors that exhibit a loss of androgen receptor dependence in castration-resistant prostate cancer (CRPC). However, there is a scarcity of prostate cancer cell line models. Tang *et al*. performed a molecular study on a number of CRPC organoids, cell lines, and patient-derived xenographs by combining sequencing techniques and transcriptomics to identify four distinct genetic subgroups of tumors. Dominant transcription factors were identified for each subgroup, with a deeper analysis of subgroup 4 leading to the identification of a chromatin-opening positive feedback loop. From these data, the authors propose that inhibitors of the transcriptional coactivators YAP and TAZ may be used to treat individuals with subgroup 4–like tumors, the second most common type of CRPC observed in this study. —LMZ